Synthesis of vertical graphene flowers as a photoelectrocatalyst for organic degradation

Fangyuan Tian[1], *Hongji Li*[1], *Mingji Li*[2] ✉

[1]*Tianjin Key Laboratory of Organic Solar Cells and Photochemical Conversion, School of Chemistry and Chemical Engineering, Tianjin University of Technology, Tianjin 300384, People's Republic of China*
[2]*Tianjin Key Laboratory of Film Electronic and Communicate Devices, School of Electronics Information Engineering, Tianjin University of Technology, Tianjin 300384, People's Republic of China*
✉ *E-mail: limingji@163.com*

Published in Micro & Nano Letters; Received on 28th November 2016; Revised on 8th December 2016; Accepted on 12th December 2016

Three-dimensional vertical graphene flowers were fabricated using a simple, low-cost, and efficient chemical vapour deposition method with $Ni(NO_3)_2$ as a catalyst precursor and methane as a carbon precursor. Graphene flowers of up to 10 μm in size with petals of two to seven layers of graphene were obtained. The growth of the vertically aligned graphene flowers was attributed to a columnar growth mechanism. Numerous micropores were observed between the flower petals and irregular mesopores were observed in the interconnected flowers. The charge-transfer resistance of a graphene flower/Ta film was 30.8 Ω. The graphene flowers acted as charge carriers, reducing the charge recombination rate and enhancing electron transport. The vertical graphene flowers showed significant photoelectrocatalytic activity for the degradation of phenol.

1. Introduction: High-performance photoelectrodes can be obtained by combining graphene with various photocatalysts [1, 2]. Materials for photocatalysts should have large surface areas and appropriate catalytic capacities. Therefore, almost all graphene materials used in photoelectrodes have been prepared from graphite oxide using wet methods [3–5]. Le *et al.* [6, 7] prepared reduced graphene oxide/carbon felt electrode as an electron-Fenton cathode. They found that the graphene enhances the electrocatalytic performance by generating hydrogen peroxide. However, graphene grown by chemical vapour deposition (CVD) is advantageous for photoelectrocatalytic (PEC) applications because it has high electrical conductivity, regular alignment, and few defects, and contains metal catalyst components [8–10]. Regrettably, current CVD graphene has been frequently overlooked in the field of photocatalysts. If graphene sheets are grown vertically, then the exposed surface area will be much greater than that of graphene grown laterally. At the same time, as CVD graphene usually contains metal catalyst particles, it is possible to achieve photocatalytic or electrocatalytic functionality without incorporating other catalyst materials. Vertical growth of graphene on a metal substrate has been rarely reported [11, 12]. Ma *et al.*[13] have reported the synthesis of standing multi-layer graphene through polymer pyrolysis CVD.

Ghosh *et al.* [14] reported the role of substrate on vertical growth of graphene in electron cyclotron resonance CVD process. The substrates guide the vertical growth of graphene nanosheets through the interfacial nanographitic layer. As graphene sheets are very thin, when a graphene sheet stands on a substrate, the edge curls, so that a large number of porous structures are formed in the graphene layer. Such structures are conducive to improving catalytic performance. The conductivity of CVD graphene and the bonding strength between the graphene layer and substrate or electrode are higher than those of graphene prepared by the wet method. Thus, vertically oriented CVD graphene is suitable as a photocatalytic electrode.

Here, we introduce a direct current (DC) arc plasma jet CVD process with nickel nitrate ($Ni(NO_3)_2$) as a catalyst precursor that produces three-dimensional (3D) vertically oriented graphene nanoflowers on Ta surfaces. These graphene nanoflowers are efficient photoelectric catalysts for the degradation of phenol under light irradiation.

2. Materials and methods: Graphene flowers were deposited on 10 × 20 mm Ta substrates using DC arc plasma jet CVD. The catalyst for this process, Ni, was produced by decomposition of $Ni(NO_3)_2$. Details of the preparation process were reported in our previous work [15]. Unlike the previous work, the growth temperature in this study was controlled at 900°C. Uniform distribution of the catalyst particles on the graphene sheets was ensured because the temperature of the plasma was the same as that of methane decomposition.

The microstructures of the graphene samples were analysed using field emission scanning electron microscopy (FESEM; JEOL JSM-6700F, Japan) and high-resolution transmission electron microscopy (HRTEM; JEOL, JEM-2100, Japan). The phase structures and composition of the samples were confirmed by X-ray diffraction (XRD; CuKα, Rigaku D/max-2500/PC, Japan) and Raman spectroscopy (Thermo Scientific DXR, YAG laser, USA). The performance of the sample as a photoelectrode was investigated by photoelectrochemical analysis (Zennium/IM6 workstation, Zahner-Elektrik, Germany) and chemical oxygen demand (COD) colorimetry (Lovibond ET99730, Germany).

3. Results and discussion: Fig. 1 shows scanning electron microscopy (SEM) images of the graphene flowers grown on the Ta substrate. The graphene flowers are up to 10 μm in size (Fig. 1*a*) and have homogeneous 3D flower-like structures with layers of petals (Fig. 1*b*). Numerous holes were formed in the graphene layers, which are observed as micropores between flower petals and irregular mesopores inside the flowers (see Fig. 2). The microstructure shown in Fig. 1*b* demonstrates that the petals consist of ultra-thin nanosheets. Cross-sectional SEM images of the sample (Figs. 1*c* and *d*) show that the graphene nanosheets are vertically aligned with a columnar growth structure. This result is consistent with a free-standing growth mechanism [11]. Further, $H_2/Ar/CH_4$ plasmas appear to play important roles in nanostructure growth [16].

Fig. 2 shows nitrogen adsorption–desorption isotherms of graphene layer. The inset shows the pore size distribution curve of sample. The graphene layers have a pore size distribution of 1.73–14.3 nm, and the most pore size is ~3.8 nm.

Figs. 3*a* and *b* show transmission electron microscopy (TEM) and HRTEM images of the petals of the graphene flowers. As the

doi: 10.1049/mnl.2016.0709

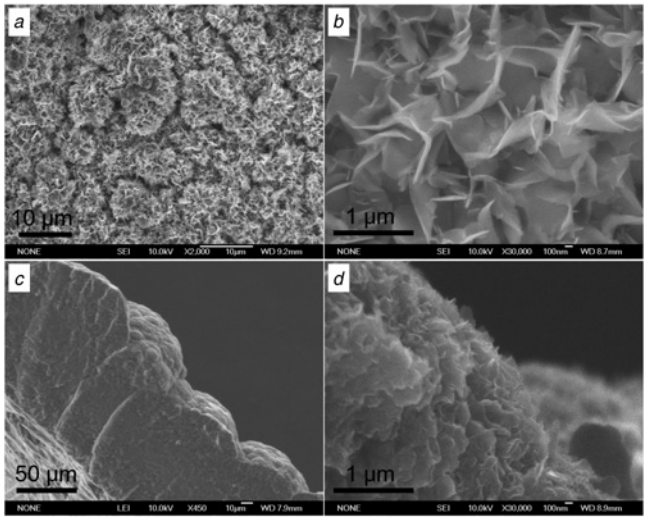

Fig. 1 *FESEM images of vertical graphene flowers*
a, *b* Top views
c, *d* Cross-sectional views of the graphene layer

theoretical thickness of the (002) plane of hexagonal graphite is 0.34 nm, the measured petal thickness of ~0.68–2.1 nm corresponds to two to seven graphite layers, indicating the ultra-thin nature of the obtained graphene flowers.

The XRD pattern of the graphene flowers on the Ta substrate exhibits peaks assignable to graphene (JCPDS Card No. 08-0415), NiO (JCPDS Card No. 65-2901), Ni (JCPDS Card No. 65-0380), TaC (JCPDS Card No. 89-3831), and Ta (JCPDS Card No. 89-5158) phases (Fig. 4*a*). The corresponding Raman spectrum, shown in Fig. 4*b*, displays three typical bands: a D band, G band, and 2D band at ~1347.5, ~1580.8, and ~2691.8 cm^{-1}, respectively. The G band is related to the in-plane vibration of sp^2 carbon atoms, whereas the 2D band is sensitive to the stacking order along the *c*-axis of the carbon atom layer in the graphite phase. The I_{2D}/I_G intensity ratio, which is known to be strongly correlated with the number of graphene layers, of the synthesised graphene flowers was 0.85, a distinctive feature of multi-layered graphene [17] and consistent with the TEM observations. The presence of the D band indicates that the average size of sp^2 carbon atoms in the sample is decreased or that defects exist [17]. The SEM, TEM, XRD, and Raman spectroscopy results all confirmed the existence of graphene on the Ta substrate with a TaC buffer layer.

A Nyquist plot and an equivalent circuit model for the graphene flower/Ta sample are shown in Fig. 5*a*. The high-frequency intercept on the real axis corresponds to the ohmic resistance of the

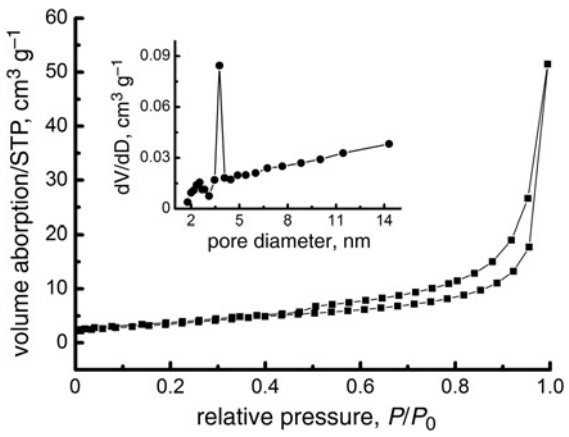

Fig. 2 *Nitrogen adsorption–desorption isotherms and corresponding pore size distribution curve (inset) of graphene layer*

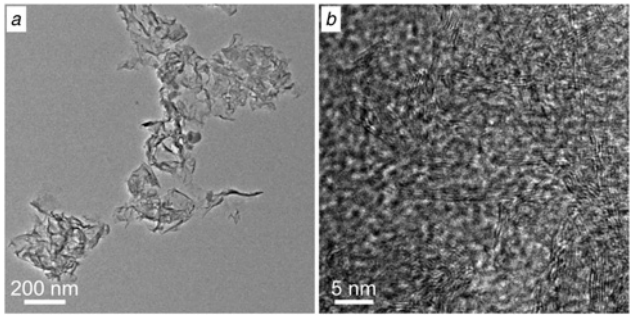

Fig. 3 *TEM and HRTEM images of graphene petal nanosheets*
a TEM images
b HRTEM images

electrolyte (R_s). In the high-frequency region, the first semicircle is related to the solid-electrolyte-interface layers, whereas the second semicircle corresponds to the charge-transfer process. The linear segment in the low-frequency region is assigned to ion diffusion within the electrode, corresponding to the Warburg element [18]. The charge-transfer resistance (R_{ct}) of the graphene flower/Ta electrode was 30.8 Ω, which is much lower than those of graphene oxide/glassy carbon electrode (GCE) (1300 Ω) [19] and chemically reduced graphene (GR)/GCE (27 Ω) [20], and relatively close to that of GR-carbon nanotube/GCE [20]. This finding suggests that the graphene flowers acted as charge carriers, reducing the charge recombination rate and enhancing the transport of electrons in the photoelectrode [21]. Fig. 5*b* shows cyclic voltammograms for the graphene flower/Ta electrode obtained at a scan rate of 100 mV s^{-1} in 0.1 M phosphate-buffered saline (PBS) solution (pH 7.0) containing 50 mg l^{-1} phenol. The peak at approximately +0.38 V is the oxidation peak of hydroquinone, while the peak at approximately +0.8 V is that of phenol. Thus, phenol was first degraded to yield benzoquinone and then benzoquinone was reduced to yield hydroquinone. When the electrode was illuminated under UV light for 10 min, the two oxidation peaks disappeared. The potential of the reduction peak decreased from 0.2 to −0.37 V with increasing UV illumination time from 0 to 60 min, indicating the degradation of phenol. The COD colorimetry results are shown in Fig. 5*c*. The removal rate of COD on the graphene flower/Ta electrode was 59.6% after 40 min of the PEC process. This result indicates that the graphene flowers have good PEC activity. The degradation efficiency of the PEC process is affected by two factors: adsorption of reactants and generation of OH^- free radicals. $Ni(NO_3)_2$ was used as the catalyst precursor in this experiment. In the presence of NiO, excited hydrogen species will reduce NiO to form metallic Ni and excited hydroxyl species ($H^* + NiO \rightarrow Ni + OH^*$) [22]. Graphene has a tunable bandgap of up to 0.21 eV [23]. Owing to its small molecular spacing, such excited hydroxyl species can easily diffuse to graphene and reoxidise it, leading to a decreased concentration of oxygen vacancies

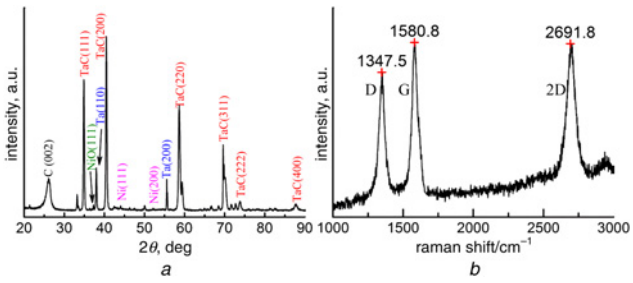

Fig. 4 *XRD pattern and Raman spectrum of the graphene flowers*
a XRD pattern
b Raman spectrum

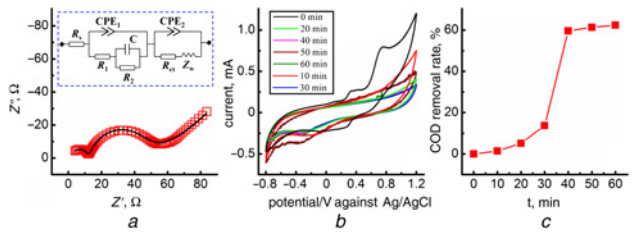

Fig. 5 *Nyquist plot and an equivalent circuit model for the graphene flower/Ta sample*
a Electrochemical impedance spectroscopy (EIS) spectrum of the graphene flower/Ta electrode in 0.1 M KCl containing 5 mM $Fe(CN)_6^{3-}/Fe(CN)_6^{4-}$ at an applied AC voltage of 0.16 V and 0.01 Hz to 100 kHz. Inset: equivalent circuit employed to fit the EIS spectrum
b Cyclic voltammograms of 50 mg l^{-1} phenol in 0.1 M PBS (pH 7) with the graphene flower/Ta electrode at different illumination times (0–60 min). Scan rate: 100 mV s^{-1}
c COD colorimetry results for the degradation of phenol by the graphene flowers

($O_V + OH^*$ G → G–O + H*). Recombination of photoinduced charge carriers releases a certain chemical energy, which is converted into heat or light energy, resulting in a higher photocatalytic activity [24]. In addition, the graphene cathode also has good stability. After 30 h of use (30 cycles), the COD removal rate of graphene cathode was almost unchanged.

4. Conclusion: The synthesis of vertically aligned graphene nanoflowers was performed using a Ni-catalysed CVD method with CH_4 as the precursor. The obtained graphene flowers had sizes of up to 10 μm with petals formed from two to seven layers of graphene. The vertically aligned growth of the graphene flowers was attributed to the columnar growth mechanism. The as-synthesised graphene flowers exhibited very rapid photodegradation of phenol, with 59.6% degradation achieved within a time interval of 40 min. This high catalytic activity is attributed to the synergistic effect of the graphene flowers and NiO/Ni catalyst. These graphene nanoflowers have the potential to be used as photoelectrocatalysts for environmental remedial applications.

5. Acknowledgments: The authors are thankful for the support from the National Natural Science Foundation of China (grant nos. 61301045 and 61401306) and the Natural Science Foundation of Tianjin City (grant no. 15JCYBJC24000), and the Youth Top-notch Talents Program of Tianjin City.

6 References

[1] Andryushina N.S., Stroyuk O.L.: 'Influence of colloidal graphene oxide on photocatalytic activity of nanocrystalline TiO_2 in gas-phase ethanol and benzene oxidation', *Appl. Catal. B, Environ.*, 2014, **148–149**, pp. 543–549
[2] Yang L., Li Z., Jiang H., *ET AL.*: 'Photoelectrocatalytic oxidation of bisphenol a over mesh of TiO_2/graphene/Cu_2O', *Appl. Catal. B, Environ.*, 2016, **183**, pp. 75–85
[3] Neelgund G.M., Oki A., Luo Z.P.: 'ZnO and cobalt phthalocyanine hybridized graphene: efficient photocatalysts for degradation of rhodamine B', *J. Colloid Interface Sci.*, 2014, **430**, pp. 257–264
[4] Morales-Torres S., Pastrana-Martinez L.M., Figueiredo J.L., *ET AL.*: 'Graphene oxide-P25 photocatalysts for degradation of diphenhydramine pharmaceutical and methyl orange dye', *Appl. Surf. Sci.*, 2013, **275**, pp. 361–368
[5] Pastrana-Martinez L.M., Morales-Torres S., Likodimos V., *ET AL.*: 'Advanced nanostructured photocatalysts based on reduced graphene oxide-TiO_2 composites for degradation of diphenhydramine pharmaceutical and methyl orange dye', *Appl. Catal. B, Environ.*, 2012, **123**, pp. 241–256
[6] Le T.X.H., Bechelany M., Lacour S., *ET AL.*: 'High removal efficiency of dye pollutants by electron-Fenton process using a graphene based cathode', *Carbon*, 2015, **94**, pp. 1003–1011
[7] Le T.X.H., Bechelany M., Champavert J., *ET AL.*: 'A highly active based graphene cathode for the electro-Fenton reaction', *RSC Adv.*, 2015, **5**, (53), pp. 42536–42539
[8] Wang B.B., Ostrikov K., van der Laan T., *ET AL.*: 'Carbon nanorods and graphene-like nanosheets by hot filament CVD: growth mechanisms and electron field emission', *J. Mater. Chem. C*, 2013, **1**, (46), pp. 7703–7708
[9] Nang L.V., Kim E.-T.: 'Low-temperature synthesis of graphene on Fe_2O_3 using inductively coupled plasma chemical vapor deposition', *Mater. Lett.*, 2013, **92**, pp. 437–439
[10] Kumar S., McEvoy N., Lutz T., *ET AL.*: 'Gas phase controlled deposition of high quality large-area graphene films', *Chem. Commun.*, 2010, **46**, (9), pp. 1422–1424
[11] Zhao J., Shaygan M., Eckert J., *ET AL.*: 'A growth mechanism for free-standing vertical graphene', *Nano Lett.*, 2014, **14**, (6), pp. 3064–3071
[12] Malesevic A., Kemps R., Vanhulsel A., *ET AL.*: 'Field emission from vertically aligned few-layer graphene', *J. Appl. Phys.*, 2008, **104**, (8), pp. 084301
[13] Ma J., Li G.-y., Chu Z.-y., *ET AL.*: 'Microstructure and growth mechanism of multi-layer graphene standing on polycrystalline SiC microspheres', *Carbon*, 2014, **69**, pp. 634–637
[14] Ghosh S., Ganesan K., Polaki S.R., *ET AL.*: 'Influence of substrate on nucleation and growth of vertical graphene nanosheets', *Appl. Surf. Sci.*, 2015, **349**, pp. 576–581
[15] Ge C., Li H., Li M., *ET AL.*: 'Synthesis of a ZnO nanorod/CVD graphene composite for simultaneous sensing of dihydroxybenzene isomers', *Carbon*, 2015, **95**, pp. 1–9
[16] Ostrikov K., Neyts E.C., Meyyappan M.: 'Plasma nanoscience: from nano-solids in plasmas to nano-plasmas in solids', *Adv. Phys.*, 2013, **62**, (2), pp. 113–224
[17] Zhu L., Jia Y., Gai G., *ET AL.*: 'Ambipolarity of large-area Pt-functionalized graphene observed in H_2 sensing', *Sens. Actuators B, Chem.*, 2014, **190**, pp. 134–140
[18] Cui X., Shan Z., Cui L., *ET AL.*: 'Enhanced electrochemical performance of sulfur/carbon nanocomposite material prepared via chemical deposition with a vacuum soaking step', *Electrochim. Acta*, 2013, **105**, pp. 23–30
[19] Zheng L., Xiong L., Li Y., *ET AL.*: 'Facile preparation of polydopamine-reduced graphene oxide nanocomposite and its electrochemical application in simultaneous determination of hydroquinone and catechol', *Sens. Actuators B, Chem.*, 2013, **177**, pp. 344–349
[20] Jaidev and Ramaprabhu S.: 'Poly(P-phenylenediamine)/graphene nanocomposites for supercapacitor applications', *J. Mater. Chem.*, 2012, **22**, (36), pp. 18775–18783
[21] Yao N., Huang J., Fu K., *ET AL.*: 'Efficiency enhancement in dye-sensitized solar cells with down conversion material ZnO: Eu^{3+}, Dy^{3+}', *J. Power Sources*, 2014, **267**, pp. 405–410
[22] Hu S., Li F., Fan Z., *ET AL.*: 'Improved photocatalytic hydrogen production property over Ni/NiO/N–TiO_2–X heterojunction nanocomposite prepared by NH_3 plasma treatment', *J. Power Sources*, 2014, **250**, pp. 30–39
[23] Freitas R.R.Q., Rivelino R., Mota F.d.B., *ET AL.*: 'Dft studies of the interactions of a graphene layer with small water aggregates', *J. Phys. Chem. A*, 2011, **115**, (44), pp. 12348–12356
[24] Wang P., Wang J., Wang X., *ET AL.*: 'One-step synthesis of easy-recycling TiO_2–rGO nanocomposite photocatalysts with enhanced photocatalytic activity', *Appl. Catal. B, Environ.*, 2013, **132–133**, pp. 452–459

doi: 10.1049/mnl.2016.0709